nature medicine

TECHNICAL REPORTS

Using the amide proton signals of intracellular proteins and peptides to detect pH effects in MRI

Jinyuan Zhou[1,2,5], Jean-Francois Payen[1,3,5], David A Wilson[4], Richard J Traystman[4] & Peter C M van Zijl[1,2]

In the past decade, it has become possible to use the nuclear (proton, ^{1}H) signal of the hydrogen atoms in water for noninvasive assessment of functional and physiological parameters with magnetic resonance imaging (MRI). Here we show that it is possible to produce pH-sensitive MRI contrast by exploiting the exchange between the hydrogen atoms of water and the amide hydrogen atoms of endogenous mobile cellular proteins and peptides. Although amide proton concentrations are in the millimolar range, we achieved a detection sensitivity of several percent on the water signal (molar concentration). The pH dependence of the signal was calibrated *in situ*, using phosphorus spectroscopy to determine pH, and proton exchange spectroscopy to measure the amide proton transfer rate. To show the potential of amide proton transfer (APT) contrast for detecting acute stroke, pH effects were noninvasively imaged in ischemic rat brain. This observation opens the possibility of using intrinsic pH contrast, as well as protein- and/or peptide-content contrast, as diagnostic tools in clinical imaging.

MRI is an extremely versatile technology that uses water content and water relaxation properties to image anatomy and function with microliter resolution. It has not been possible, however, to use this water signal to assess pH effects. Efforts to develop exogenous contrast agents for pH detection using water resonance are ongoing[1–6] but still remain at the *in vitro* stage. A method for imaging pH by endogenous contrast would allow immediate, noninvasive clinical use of this important physiological indicator as part of a multimodality MRI exam. Although phosphorus (^{31}P) magnetic resonance spectroscopy (MRS) can assess pH[7], this approach has low spatial resolution (20–30 ml) and is not available on standard clinical equipment, which is limited predominantly (>99%) to proton (^{1}H) studies. We hypothesized that intrinsic pH-sensitive proton MRI should be possible by exploiting the exchange contact between amide protons of mobile intracellular proteins and peptides and the protons of water molecules. Studies of protein solutions[8–10] have shown that the signal intensities and line widths of the amide proton resonances depend on the hydrogen exchange rates. This exchange rate is base-catalyzed for pH values above ~5, and are thus proportional to the hydroxyl ion concentration and exponentially proportional to pH[8–10]. The backbones of proteins and peptides have amide resonances around 8.3 parts per million (p.p.m.) in the proton spectrum. A composite resonance is present around 8.3 ± 0.5 p.p.m. in the *in situ* proton spectra of cancer cells and cat brain, the signal intensity of which is sensitive to pH changes[11]. If this resonance is due to amide hydrogen atoms, it should be possible to conduct pH-sensitive imaging as hypothesized above.

RESULTS

Confirmation of amide ^{1}H resonance identity

To verify that the composite resonance at 8.3 p.p.m. is caused by amide protons, we did an *in situ* rat brain spectroscopy experiment in which water magnetization was selectively labeled and its transfer properties were monitored as a function of time after labeling (mixing time, t_m). In such water exchange (WEX) experiments[10], signals originate from mobile molecular species that engage in transfer of magnetization with water by either chemical exchange or intermolecular nuclear Overhauser enhancement (NOE)[12]. After such transfers, intramolecular NOE effects can become visible in larger, slower-moving but mobile macromolecules. Proton signals of exchangeable hydrogen atoms are only visible at their expected resonance frequency if exchange is slow on the time-scale of the MRI measurement (exchange rate constant $k <$ frequency separation between the proton signals of water and the particular hydrogen). This excludes most -OH, -SH, amine and amino protons from detection because they exchange too quickly and have an average frequency coinciding with the water resonance. Thus, amide protons of mobile proteins and peptides (6–10 p.p.m.) and aliphatic signals (0–3.5 p.p.m.) from mobile macromolecules (proteins, larger peptides and some lipids) are visible, whereas aliphatic resonances of smaller molecules, such as brain metabolites, are not. The solid-like spectrum of importance in conventional magnetization transfer imaging experiments[13,14] is too broad to be detected (120–200 kHz). *In situ* WEX spectra (**Fig. 1a**,**b**) at short t_m values show fast appearance of the resonance at 8.3 p.p.m. and measured exchange rates (**Fig. 2**) that are in the typical range for amide protons. At longer values of t_m, signals appear in the aliphatic resonance range (0–3.5 p.p.m.) at the time scale of a typical intramolecular protein NOE

[1]Division of MRI Research, Department of Radiology, Johns Hopkins University School of Medicine, 217 Traylor Building, 720 Rutland Avenue, Baltimore, Maryland 21205, USA. [2]F.M. Kirby Research Center for Functional Brain Imaging, Kennedy Krieger Institute, Baltimore, 707 N. Broadway, Maryland 21205, USA. [3]Department of Anesthesiology, The Grenoble University School of Medicine, 38000 Grenoble, France. [4]Department of Anesthesiology and Critical Care Medicine, Johns Hopkins University School of Medicine, 1408 Blalock Building, 600 N. Wolfe Street, Baltimore, Maryland 21287, USA. [5]These authors contributed equally to this work. Correspondence should be addressed to P.C.M.v.Z. (pvanzijl@mri.jhu.edu) or J.Z. (jzhou@mri.jhu.edu).

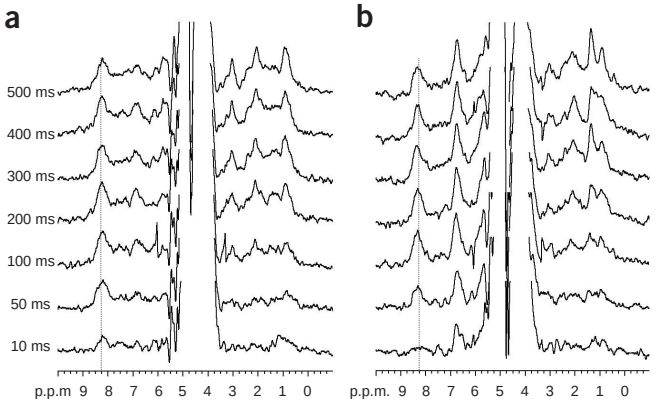

Figure 1 Water exchange (WEX) spectra for rat brain as a function of time after radiofrequency labeling of water magnetization (mixing time t_m). (**a**) Normocapnia. (**b**) Postmortem. Note the early appearance of signals around 8.3 p.p.m. (fast exchange transfer) and the subsequent slower label transfer to the (aliphatic) protons at lower frequency, which is in line with measured effects in protein solution[10]. The aliphatic spectra closely resemble protein spectra measured *in vivo* using other methods[15,16]. Resonance at 1.3 p.p.m. became much more pronounced under postmortem conditions. We attributed this to a mobile lipid component, known to increase during ischemia[27].

transfer[12], indicating a substantial mobile protein contribution to the WEX spectra. The signs of the intramolecular NOE effects and exchange peaks are equal, whereas those of intermolecular NOE are opposite, excluding a major contribution of the latter to the spectrum. The resulting aliphatic spectra closely resemble the frequency-dependent shape of mobile protein spectra previously detected in the rat brain using alternative approaches[15,16]. Additional evidence of macromolecular origin comes from the fact that all peaks (except water) decayed quickly with echo time (data not shown). Although the WEX spectra are insensitive to lactate, we verified that the 1.3-p.p.m. resonance was not lactate by going to longer TE (136 ms, where lactate should give an inverted resonance), which showed no signals (data not shown). The integrals of the amide proton signals at longer values of t_m are comparable *in vivo* and postmortem, but the build-up rate of the peak differs (see Fig. 2).

Characterizing APT

The concentration of cellular mobile proteins and peptides is in the millimolar range and detection via the water resonance would provide a sensitivity enhancement of 100- to 1,000-fold. We approached this in a manner inverse to that of WEX spectra[2,4] by selectively labeling amide protons through radiofrequency irradiation at 8.3 p.p.m. and by imaging water after several seconds of transfer. This proton exchange saturation transfer approach[2,17] is especially suitable for amide protons[4], which have a favorable exchange rate range (10–300 s^{-1}) that is rapid but retains distinct resonance identity at intermediate and high magnetic field strength, thus allowing selective irradiation under physiological conditions. It is not easy to show APT effects on water signal in tissues because of several confounding MRI phenomena. First, there is a large magnetization transfer effect between solid-like macromolecular structures and cellular water[13,14]. In addition, blood oxygen level–dependent (BOLD) MRI effects occur during physiological adjustments such as hypercapnia (increased CO_2 level), ischemia or cardiac arrest. **Figure 3a,b** shows magnetization transfer spectra ($n = 7$), in which radiofrequency saturation effects on water are plotted as a function of saturation frequency offset relative to water. In addition to direct water saturation and conventional magnetization transfer effects, several interesting features indicate the existence of APT effects. First, there is a very small dip at a frequency difference of 3.5 p.p.m. from water, corresponding to about 8.3 p.p.m. in the WEX spectra, where amide protons resonate. Second, when comparing the *in vivo* and postmortem results (**Fig. 3a**), the magnetization transfer curves coincide on the negative-offset side of water, but not on the positive-offset side, where the exchangeable protons resonate. This supports the notion that decreased pH in postmortem brain leads to a decreased proton exchange rate, resulting in reduced saturation transfer. During hypercapnia (**Fig. 3b**), an upward shift of the total magnetization transfer curve is visible, which we attribute to the BOLD effect, where increased blood flow lengthens the relaxation time T_2, thus narrowing the direct saturation curve of water.

To selectively assess the effects of APT without conventional magnetization transfer interference, direct water saturation and BOLD effects, we used a magnetization transfer ratio asymmetry parameter, $MTR_{asym} = S_{sat} / S_0$ (negative offset) – S_{sat} / S_0 (positive offset). If magnetization transfer effects were symmetric with respect to the water resonance, APT effects would give a positive magnetization transfer difference. The measured MTR_{asym} curves (**Fig. 3c**) show a magnetization transfer difference that is slightly positive at first and becomes negative at higher offset. This finding supports a report that magnetization transfer effects are asymmetric with respect to the water resonance, with a center frequency in the aliphatic range[18]. When we did an additional series of experiments with extended irradiation range (**Fig. 3d**; $n = 3$), MTR_{asym} became constant at about –3% for offsets above 5 p.p.m., where the exchangeable proton region ends. This has important interpretive consequences, vide infra. The curve for offsets 0–5 p.p.m. from water has an offset-dependent shape that depends on the inherent MTR_{asym} of the solid-phase magnetization transfer effect (MTR'_{asym}), as well as on the proton transfer ratio (PTR) of the exchangeable protons, according to the equation

$$MTR_{asym}\,(\text{offset}) = MTR'_{asym}\,(\text{offset}) + PTR\,(\text{offset})$$

Using the difference between MTR_{asym} curves for different physiological perturbations, the change in proton transfer ratio (ΔPTR) can be assessed under the assumption that MTR'_{asym} remains unaltered. The postmortem results (**Fig. 3e,f**) show a maximum change at an offset of 3.5 p.p.m. from water. This corresponds exactly to the amide proton frequency, and the effect has the expected sign for a pH decrease. Assuming complete amide proton saturation and negligible back-exchange from saturated water, the PTR for the amide protons ($APTR$) is derived[4] as

$$APTR = \frac{k[\text{amide proton}]}{2[H_2O]R_{1w}}\left(1 - e^{-R_{1w}t_{sat}}\right) \qquad (1)$$

where R_{1w} is the spin-lattice relaxation rate and t_{sat} is the saturation time (4 s). Based on the appearance of the MTR_{asym} images, we need to assume similar APT effects for white and gray matter and use an average tissue R_{1w} of 0.714 s^{-1} at 4.7 T (ref. 19) and an average water content of 0.84 ml water per ml brain[20] (obtained using a density of 1.05 g per ml tissue[21]).

Equation (1) indicates that APT effects depend on the water content of tissue. Data at 1–1.5 T (refs. 20, 22) show that R_{1w} and water content are directly related and inversely proportional, the relative effect on R_{1w} being about 2.5–3 times larger than that on water con-

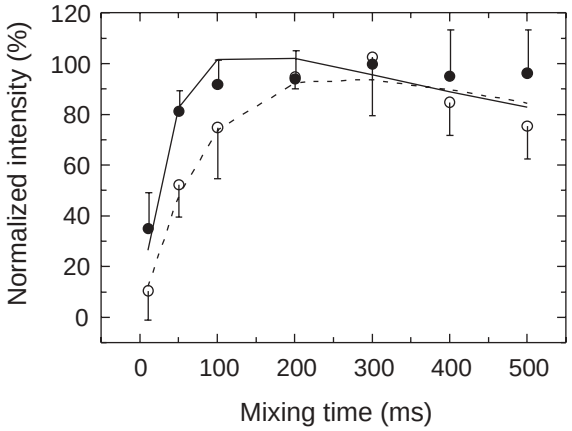

Figure 2 Fitting of exchange rates using the dependence of the amide proton signal integral ($n = 5$) from WEX spectra on mixing time (t_m). ● and —, normocapnia *in vivo*; ○ and – – –, postmortem. Integrals were normalized to the normocapnic value at $t_m = 300$ ms. Exchange rates (k) were 28.6 ± 7.4 s^{-1} and 10.1 ± 2.6 s^{-1} for *in vivo* and postmortem, respectively. No change in amide intensity at $t_m = 300$ ms is seen in the first 2 h postmortem, from which we concluded that this rate change was caused by the pH change upon death.

tent. Although these effects partially compensate each other in the equation, measurement of R_{1w} is an important additional experiment for quantification. We did not measure R_{1w} in our original series of experiments, but we did an additional study ($n = 3$) that resulted in $R_{1w} = 0.719 \pm 0.045$ *in vivo* and 0.726 ± 0.036 at the 45-min postmortem time point typically used for our earlier data. This shows negligible R_{1w} changes for the time frame used in our studies. An additional impression of changes in R_{1w} can be obtained from the shape of the direct water-saturation effect in the magnetization transfer curve, which should have similar water-content and R_{1w} effects. No changes between *in vivo* and postmortem are visible on the low-frequency side of the magnetization transfer curve (**Fig. 3a**), indicating only limited changes in R_{1w}. Further evidence of the limited effect of water content on magnetization transfer comes from another study[23] showing that 2–3% changes in tissue water content during hypertensive cardiomyopathy affect the relaxation rates R_{1w} and R_{2w}, but not MTR. This effect is further illustrated by ischemia and postmortem experiments (**Fig. 4a,b**) showing a narrowed magnetization transfer curve for increased edema (5 h versus 2 h), but negligible change in the MTR_{asym} curve at the amide frequency.

When interpreting APT data, it is important to keep in mind that the amide content of tissues may change depending on pathology (when tumors are compared with normal tissue, for example). Also, cerebrospinal fluid (CSF, which has long T_1 and T_2) shows a narrowed magnetization transfer curve (**Fig. 3g**) and an MTR_{asym} curve (**Fig. 3h**) with a negligible effect at 3.5 p.p.m. offset. Differences between gray and white matter may also exist, but these two tissue types are difficult to distinguish in rat brain MTR_{asym} echo-planar images. The postmortem amide-signal integral (**Fig. 2**) did not

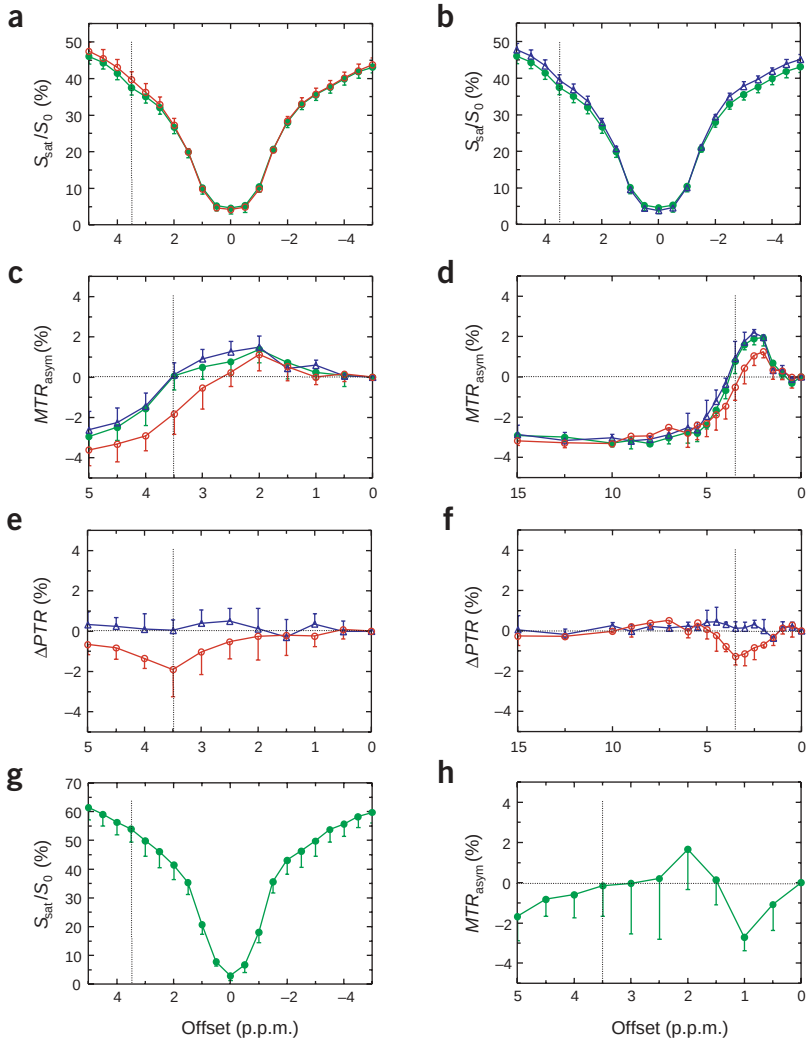

Figure 3 *In situ* APT effects during normocapnia (green), hypercapnia (blue) and cardiac arrest (red). (**a**,**b**) Magnetization transfer spectra, giving the ratio of water signal intensities with (S_{sat}) and without (S_0) saturation. Five regions of interest covering the whole brain (fronto-parietal cortex, inferior colliculus and cerebellum) were chosen and averaged. Signal attenuation was mainly due to direct water saturation close to the water frequency and the solid-like magnetization transfer effect over the whole spectral range. There is a small APT-based dip at offset 3.5 p.p.m. during normocapnia (**a**,**b**) and hypercapnia (**b**), which disappears after cardiac arrest (**a**). This 3.5-p.p.m. offset corresponds to the amide frequency around 8.3 p.p.m. in the WEX spectra (**Fig. 1**). (**c**,**d**) MTR_{asym} spectra for 5-p.p.m. (**c**; $n = 7$) and 15-p.p.m. (**d**; $n = 3$) offset ranges. (**e**,**f**) DPTR spectra for 5-p.p.m (**e**) and 15-p.p.m. (**f**) offset ranges. Postmortem changes are only visible in the 0- to 5-p.p.m. offset range from water, corresponding to the exchangeable proton range in WEX spectra. (**g**,**h**) Magnetization transfer (**g**) and MTR_{asym} (**h**) spectra in regions containing CSF (light green). In contrast to the magnetization transfer curve for tissue, the CSF magnetization transfer curve is narrow and shows negligible asymmetry features, with large standard deviations at 3.5 p.p.m. offset.

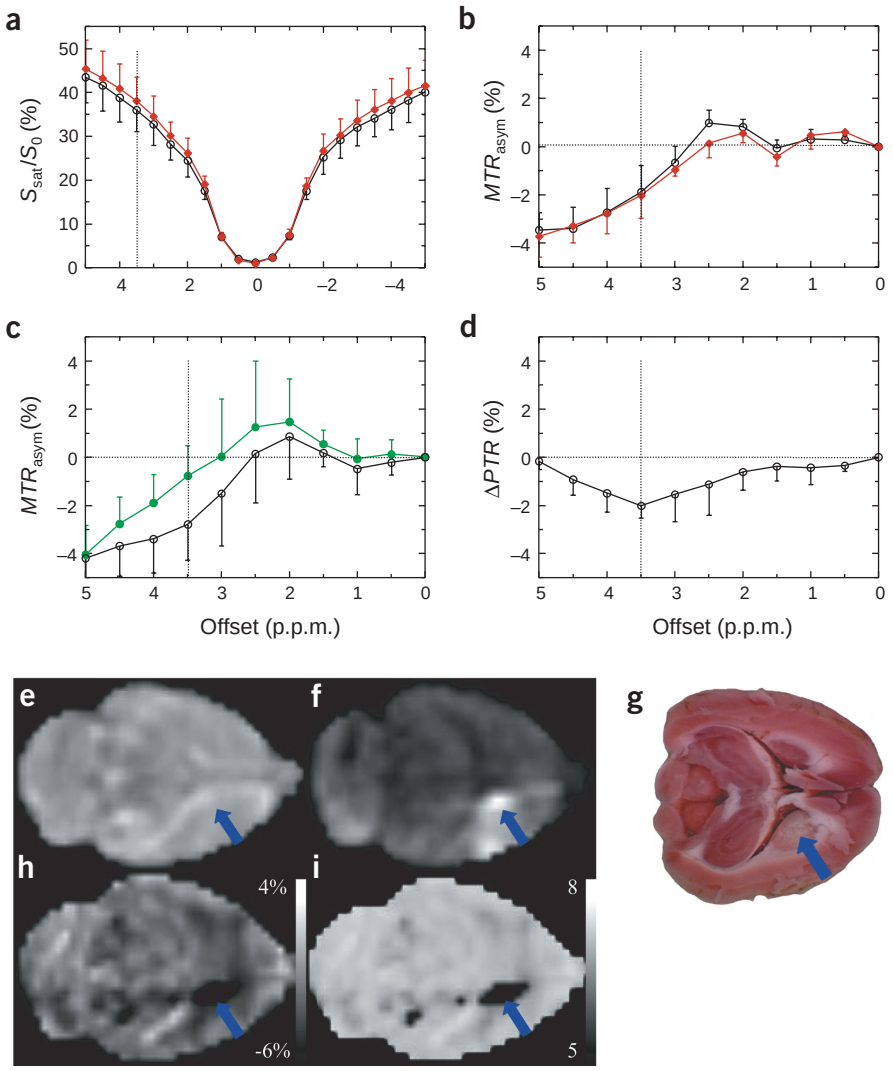

Figure 4 APT effects during focal ischemia in the rat brain. (**a**,**b**) Comparison of ipsilateral magnetization transfer effects in the caudate nucleus at 2 h of ischemia (●; $n = 2$) with 5 h post-ictus (4 h ischemia and 1 h postmortem; ●), showing noticeable increase in water content (narrower magnetization transfer curve (**a**) without changes in MTR_{asym} at 3.5 p.p.m. offset (**b**). (**c**,**d**) Ipsilateral (●) and contralateral (●) MTR_{asym} and ΔPTR data for the caudate during ischemia ($n = 7$). MTR_{asym} spectra (**c**) compare very well with those for normocapnic and postmortem brain (**Fig. 3c**), and the magnitude of ΔPTR at the offset of 3.5 p.p.m. (**d**) is similar for the normocapnia/postmortem case. (**e**–**i**) Comparison of T_2-weighted (**e**), isotropic diffusion–weighted (**f**), 2,3,5-triphenyltetrazolium chloride (TTC)-stained (**g**), absolute MTR_{asym} (3.5 p.p.m; **h**) and absolute pH images (**i**) for ischemic rat brain. The MTR_{asym} (3.5 p.p.m.) images, which are pH-weighed were acquired using frequency-labeling offsets of ± 3.5 p.p.m. (40 scans). B_0 inhomogeneity was corrected using field maps for the same animal, in combination with the magnetization transfer data acquired at the offsets of ± 3.0 and ± 4.0 p.p.m. (16 scans). The area of ischemia (arrow) visible on the right side of the images is located in the caudate nucleus, a region that commonly becomes affected after MCAO. No effect of ischemia was visible on the T_2-weighted image (**e**), but the pH-sensitive images (**h** and **i**) show the ischemic region, as confirmed by the diffusion-weighted image (**f**), and histology, which was acquired 8 h later (**g**).

change significantly with respect to normocapnia, indicating that the mobile protein and peptide content remained constant during this early period. Assuming negligible changes during the first 2 h postmortem for the product $[H_2O]R_{lw}$ and the small exponential relaxation term of equation (1), the total amide proton concentration of all proteins and peptides that constitute the broad 8.3-p.p.m. resonance can be calculated. Using the determined $\Delta APTR$ value of –1.90%, a water concentration of 55 M, and the measured exchange rates at normocapnia and postmortem (**Fig. 2**), the total amide proton concentration is 71.9 mM, giving $APTR$ values of 2.94% at normocapnia and 1.04% postmortem.

APT pH calibration

To calibrate the exchange-rate changes in terms of intracellular pH changes, we used phosphorus (^{31}P) spectroscopy to determine intracellular pH values. This is valid assuming that the inorganic phosphate species used in phosphorus spectroscopy experience the same intracellular environment as amide protons. The pH values ($n = 7$; mean ± s.d.) were 7.11 ± 0.13 at normocapnia, 6.97 ± 0.06 during hypercapnia and 6.66 ± 0.10 postmortem. Although there was a trend towards a small $APTR$ reduction during hypercapnia, these changes were not significant. Also, it was difficult to retain physiological stability during the time-consuming (see Methods) measurement of exchange rates with WEX spectra during hypercapnia. Therefore, we used only the postmortem results for the pH calibration. Using the fact that amide proton exchange is predominantly base-catalyzed[8–10] at pH > 5, it can be derived that:

$$k = k_{base}\,[OH] = k_{base} \times 10^{pH - pK_w} = 5.57 \times 10^{pH - 6.4} \qquad (2)$$

in which a value of $5.57 \times 10^9\ s^{-1}$ was obtained for the base-catalyzed exchange rate (k_{base}) by fitting the *in vivo* and postmortem exchange rates versus pH, using $pK_w = 15.4$ at 37 °C (ref. 24). Using this, an amide pK value of 17.2 is calculated, in good agreement with literature values. Thus, using the amide concentration of 71.9 mM, we have $APTR = 5.73 \times 10^{pH-9.4}$ for rat brain tissue.

It is important to understand the many assumptions (see previous section), data (amide content is constant and APT is independent of small water-content changes) and specific approaches underlying this result. The deduced equation is based on negligible effects of temperature on exchange rate. In addition, our calibration using limited points is prone to large inaccuracies, especially in view of the standard deviations of the pH and rate measurements. To check whether an *in vitro* calibration using more points was possible, we acquired whole-brain extracts of several rats and performed WEX and magnetization transfer measurements as a function of pH at 37 °C. In that experiment, the spectral appearance of the composite

amide resonance was different from that seen *in vivo*, and the exchange-rate dependence on pH was much lower, which is not surprising as many proteins and peptides may have been lost in the extraction process. Thus, our present approach seems to be the only one possible. A group of proteins has been reported to contribute to the rat brain *in vivo* spectrum[15]. We investigated 2-mM solutions of the most abundant proteins; of these, histone gave an amide proton exchange rate of the correct order of magnitude, with a pH dependence at 37 °C ($k = 39.6 \pm 2.7\ s^{-1}$ at pH 7.05 and $k = 22.5 \pm 2.8\ s^{-1}$ at pH 6.66) that is similar to that of amide protons *in situ*. We therefore used this protein to check whether temperature effects on exchange rate would influence the postmortem calibration. The results for a pH 6.76 solution ($k = 23.2 \pm 3.8\ s^{-1}$ at $T = 29.9 \pm 0.1$ °C; $k = 23.6 \pm 6.8\ s^{-1}$ at $T = 33.4 \pm 0.4$ °C; and $k = 25.7 \pm 2.1\ s^{-1}$ at $T = 37.4 \pm 0.1$ °C) indicate that a postmortem temperature range of 1–3 °C should not appreciably alter k compared with the effect of pH. One factor that may change the exchange rate is the protein concentration, but the results in **Figure 2** show a negligible postmortem change in amide proton concentration, indicating that this concentration effect is expected not to be significant during the initial stages of ischemia.

Imaging of pH changes during ischemia

Despite the availability of many MRI modalities, it is presently difficult to assess the viability of the ischemic penumbra (a zone of reduced flow around the ischemic core) in acute stroke patients. Impaired oxygen metabolism and concomitant pH changes are crucial to the progress of the ischemic cascade, and the possibility of noninvasive detection of pH changes will aid the treatment decision. To establish the feasibility of pH-weighted MRI detection of ischemia using APT, we studied middle cerebral artery occlusion (MCAO) in seven rats (**Fig. 4a–g**). Similar to the *in vivo* and postmortem case (**Fig. 3c**), comparison of the MTR_{asym} spectrum between ischemic and contralateral regions shows a reduction in intensity for the 2- to 5-p.p.m. offset range (**Fig. 4c**). Again the largest ΔPTR effect (–2.01 ± 0.51%; caudate) is at 3.5 p.p.m. from water (**Fig. 4d**). Imaging of MTR_{asym} (3.5 p.p.m.; **Fig. 4h**) shows a strong negative effect in the caudate that corresponds well with the ultimate injury found during histological staining (**Fig. 4g**).

If the assumptions and conditions underlying the calibration procedure in the previous section hold true during ischemia, it should be possible to generate an absolute pH image. In light of reported limited water-content increases (4–8%; ref. 20) and R_{1w} decreases (10–15% at 4.7 T; ref. 25) during 1.5–3 h of focal ischemia, we expect these parameters to have only a limited influence on APT. This has been confirmed by data showing only a 2–4% increase in MTR[25,26] at such time post-ictus. Further evidence comes from our data showing negligible MTR_{asym} effects (**Fig. 4b**) at the amide frequency between 2 and 5 h of ischemia, even when the effects of edema for this situation can be seen in the magnetization transfer spectra (**Fig. 4a**). The pH map (**Fig. 4i**) confirms the possibility of pH quantification by showing a homogeneous pH of 7.0–7.4 in normal brain and a lowered pH in the caudate. Some artifacts can be seen in regions containing CSF, where the signal-to-noise in the MTR_{asym} data is low as MTR_{asym} approaches zero (**Figs. 3g,h** and **4h**). The ischemic pH varied largely between animals, giving an average of 6.52 ± 0.32 ($n = 7$) in the caudate.

DISCUSSION

We developed a new tissue-water-based MRI contrast reflecting content and exchange properties of cellular amide protons. As a consequence of the need for both selective irradiation of the amide protons and rapid amide exchange that remains slow on the NMR time scale, the method will work better at higher magnetic fields. When studying APT effects, magnetization transfer curves may shift depending on the local field in tissue, so a field-inhomogeneity shift correction is needed (see Methods). When using APT, it is important to keep in mind that the contrast is magnetization transfer–based and depends on many parameters:

$$MTR_{asym}(3.5\,ppm) = MTR'_{asym}(3.5\,ppm) + \frac{[\text{amide proton}]}{[\text{water proton}]} \cdot \frac{\left(1 - e^{-R_{1w} t_{sat}}\right)}{R_{1w}} \cdot k_{base} \cdot 10^{pH - pK_w}$$

The second term is the *APTR*, and base-catalyzed amide exchange is assumed in the pH term. Thus, APT contrast reflects relative changes in pH, amide content, water content and R_{1w}. Quantification of single parameters can only be achieved under the correct conditions and will depend on the tissue type. Using a simple *in vivo* and postmortem calibration under conditions of negligible changes in amide proton content and limited changes in water content (and thus R_{1w}), absolute pH images could be generated. An *APTR* change of 50–70% was found for a pH change of about 0.5 units, indicating that it should be possible to observe pH changes on the order of 0.2 units or larger in MTR_{asym} (3.5 p.p.m.) and pH images. The relaxation rate R_{1w} reports on water content, and its simultaneous measurement will improve quantification. Another possible use for APT contrast is imaging of protein and peptide content. Potential applications are noninvasive cancer imaging (the concentration of proteins and peptides is often altered in tumors) and magnetic resonance histology–based protein content staining.

METHODS

Animal preparation. Animal experiments were approved by the Johns Hopkins University Institutional Animal Care and Use Committee. Sprague-Dawley rats (350–500 g; $n = 22$) were anesthetized with halothane (4% induction, 1.5% during surgery). Femoral artery was catheterized to monitor blood pressure and collect blood samples, and a tracheotomy was performed. During MRI, inhaled anesthesia was changed to pentobarbital (6 mg per kg per h, delivered by intraperitoneal cannula). The animal was relaxed with pancuronium bromide (0.2 mg per kg per h intraperitoneally). For hypercapnia, inhaled arterial CO_2 levels were mechanically adjusted and allowed to stabilize for 15 min. Arterial blood gases and pH were analyzed with a 248 pH/Blood Gas Analyzer (Chiron Diagnostics). Body temperature was maintained at 37.5 ± 0.5 °C using a heating pad. Anesthetized rats were euthanized using saturated KCl.

Phantoms. Solutions of histone (Sigma) were made using physiological buffer. The pH was measured using a pH meter; temperature was maintained using a water bath and was measured before and after magnetic resonance spectroscopy using a thermocouple.

MRI. Experiments were done on a horizontal-bore, 4.7-T General Electric CSI scanner using a 3-cm surface coil. In the magnetization transfer experiments, a train of 400 Gaussian pulses (length 6.6 ms, flip angle 180°, delay 3.4 ms, total duration 4 s, average radiofrequency power 50 Hz) was used, followed by four-shot, spin-echo, echo-planar imaging acquisition (repetition time (TR) 10 s, echo time (TE) 50 ms, 64 × 64, field of view (FOV) 40 × 40 mm^2). The axial slice was located 4 mm from the brain top (thickness 2 mm for *in vivo* and postmortem) or at the caudate nucleus (thickness 4 mm for ischemia). One image was acquired per offset, starting from the water (0 Hz, on-resonance) and subsequently alternating between positive and negative offsets. An unsaturated image was acquired for all physiological states. Possible frequency shifts in the magnetization transfer curves, such as those caused by field inhomogeneity, may strongly affect the APT data. To correct for this, signal intensities as a function of offset (magnetization transfer spectrum) were fitted on a pixel-by-pixel basis using a twelfth-order polynomial. The actual water reso-

nance was assumed to be at the frequency with the lowest signal intensity of the interpolated fitted curve. After fitting, the measured curve minima (resolution 1 Hz) were shifted to coincide between voxels.

^{1}H MRS. For WEX spectroscopy[10], water was selectively labeled by the pulse unit (90° (spatially selective) – G_1 – 180° (water-selective) – G_1 – 90° (spatially selective)), after which label transfer was detected as a function of mixing time ($-t_m$ – 90° (spatially selective) –detection). Spatial selection was improved with outer-volume suppression. Parameters were as follows: volume size, 16 × 12 × 4 mm^3, set at 4 mm from the top of the brain; spectral width, 3,000 Hz; 1,024 points; 256 scans; TR 4 s; TE 8 ms. The peak at 0.916 p.p.m. was used as a chemical shift reference. Exchange rates were determined by three-parameter fitting to the two-site exchange equation[10], $S = [S_0k/(R_{1NH} + k - R_{1w})][\exp(-R_{1w}t_m) - \exp(-(R_{1NH} + k)t_m)]$. This procedure can fit a large range of exchange rates and is necessary to define constraints. For the rat brain, we assumed base-catalyzed exchange and used the pH values determined *in vivo* and postmortem by ^{31}P spectroscopy to restrict the exchange-rate ratio, as defined by equation (2). In the first fitting iteration, equal S_0 and R_{1NH} values were assumed *in vivo* and postmortem. In the second iteration, we used equal S_0 (after normalization and initial fitting, the average S_0 over all *in vivo* and postmortem data was used) and equal R_{1NH} values for all animals. For the protein samples, we used a two-parameter fit and assumed $k >> R_{1NH}$ and $R_{1w} = 0.4\ s^{-1}$ at 4.7 T.

^{31}P spectroscopy. A double-tuned (^{31}P/^{1}H) coil was used. Localized brain spectra were acquired using three-dimensional outer-volume suppression followed by hard pulse excitation. Insignificant skull muscle signal contamination was confirmed by disappearance of phosphocreatine signal about 15 min postmortem. Ischemic muscle can display phosphocreatine for hours. Intracellular pH (pH_i) was calculated from the chemical shift difference (δ) between inorganic phosphate and phosphocreatine using $pH_i = 6.75 + \log[(\delta - 3.26)/(5.70 - \delta)]$.

ACKNOWLEDGMENTS

We thank S. Mori, P. Barker, J. Pekar, X. Golay and N. Goffeney for helpful discussions; J. Klaus and M. Piper for animal preparation; and V. Chacko for technical assistance. This work was supported by the National Institutes of Health/National Institute of Neurological Disorders and Stroke (NS31490), the Whitaker Foundation, the French Defense Ministry and the French Society of Anesthesia and Critical Care.

COMPETING INTERESTS STATEMENT

The authors declare competing financial interests (see the Nature Medicine website for details).

Received 12 August 2002; accepted 5 June 2003
Published online 20 July 2003; doi:10.1038/nm907

1. Helpern, J.A., Curtis, J.C., Hearshen, D., Smith, M.B. & Welch, K.M.A. The development of a pH-sensitive contrast agent for NMR ^{1}H imaging. *Magn. Reson. Med.* **5**, 302–305 (1987).
2. Ward, K.M., Aletras, A.H. & Balaban, R.S. A new class of contrast agents for MRI based on proton chemical exchange dependent saturation transfer (CEST). *J. Magn. Reson.* **143**, 79–87 (2000).
3. Ward, K.M. & Balaban, R.S. Determination of pH using water protons and chemical exchange dependent saturation transfer (CEST). *Magn. Reson. Med.* **44**, 799–802 (2000).
4. Goffeney, N., Bulte, J.W.M., Duyn, J., Bryant, L.H. & van Zijl, P.C.M. Sensitive NMR detection of cationic-polymer-based gene delivery systems using saturation transfer via proton exchange. *J. Am. Chem. Soc.* **123**, 8628–8629 (2001).
5. Zhang, S., Winter, P., Wu, K. & Sherry, A.D. A novel europium(III)-based MRI contrast agent. *J. Am. Chem. Soc.* **123**, 1517–1578 (2001).
6. Aime, S. *et al.* Paramagnetic lanthanide(III) complexes as pH-sensitive chemical exchange saturation transfer (CEST) contrast agents for MRI applications. *Magn. Reson. Med.* **47**, 639–648 (2002).
7. Moon, R.B. & Richards, J.H. Determination of intracellular pH by ^{31}P magnetic resonance. *J. Biol. Chem.* **248**, 7276–7278 (1973).
8. Englander, S.W., Downer, N.W. & Teitelbaum, H. Hydrogen exchange. *Annu. Rev. Biochem.* **41**, 903–924 (1972).
9. Liepinsh, E. & Otting, G. Proton exchange rates from amino acid side chains-implication for image contrast. *Magn. Reson. Med.* **35**, 30–42 (1996).
10. Mori, S., Abeygunawardana, C., Berg, J.M. & van Zijl, P.C.M. NMR study of rapidly exchanging backbone amide protons in staphylococcal nuclease and the correlation with structural and dynamic properties. *J. Am. Chem. Soc.* **119**, 6844–6852 (1997).
11. Mori, S., Eleff, S.M., Pilatus, U., Mori, N. & van Zijl, P.C.M. Proton NMR spectroscopy of solvent-saturable resonance: a new approach to study pH effects *in situ*. *Magn. Reson. Med.* **40**, 36–42 (1998).
12. Wuthrich, K. in *NMR of proteins and nucleic acids* (John Wiley & Sons, New York, 1986).
13. Wolff, S.D. & Balaban, R.S. Magnetization transfer contrast (MTC) and tissue water proton relaxation *in vivo*. *Magn. Reson. Med.* **10**, 135–144 (1989).
14. Henkelman, R.M., Stanisz, G.J. & Graham, S.J. Magnetization transfer in MRI: a review. *NMR Biomed.* **14**, 57–64 (2001).
15. Kauppinen, R.A., Kokko, H. & Williams, S.R. Detection of mobile proteins by proton nuclear magnetic resonance spectroscopy in the guinea pig brain *ex vivo* and their partial purification. *J. Neurochem.* **58**, 967–974 (1992).
16. Behar, K.L. & Ogino, T. Characterization of macromolecule resonances in the ^{1}H NMR spectrum of rat brain. *Magn. Reson. Med.* **30**, 38–44 (1993).
17. Wolff, S.D. & Balaban, R.S. NMR imaging of labile proton exchange. *J. Magn. Reson.* **86**, 164–169 (1990).
18. Pekar, J. *et al.* Perfusion imaging with compensation for asymmetric magnetization transfer effects. *Magn. Reson. Med.* **35**, 70–79 (1996).
19. Zhou, J., Mori, S. & van Zijl, P.C.M. FAIR excluding radiation damping (FAIRER). *Magn. Reson. Med.* **40**, 712–719 (1998).
20. Lin, W. *et al.* An absolute measurement of brain water content using magnetic resonance imaging in two focal cerebral ischemic rat models. *J. Cereb. Blood Flow Metab.* **20**, 37–44 (2000).
21. Torack, R.M., Alcala, H., Gado, M. & Burton, R. Correlative assay of computerized cranial tomography (CCT), water content and specific gravity in normal and pathological postmortem brain. *J. Neuropathol. Exp. Neurol.* **35**, 385–392 (1976).
22. Fatouros, P.P., Marmarou, A., Kraft, K.A., Inao, S. & Schwarz, F.P. *In vivo* brain water determination by T_1 measurement: effect of total water content, hydration fraction, and field strength. *Magn. Reson. Med.* **17**, 402–413 (1991).
23. Scholz, T.D., Ceckler, T.L. & Balaban, R.S. Magnetic transfer characterization of hypertensive cardiomyopathy: significant of tissue water content. *Magn. Reson. Med.* **29**, 352–357 (1993).
24. Covington, A.K., Robinson, R.A. & Bates, R.G. The ionization constant of deuterium oxide from 5 to 50 °C. *J. Phys. Chem.* **70**, 3820–3824 (1966).
25. Makela, H.I., Kettunen, M.I., Grohn, O.H. & Kauppinen, R.A. Quantitative $T_{1\rho}$ and magnetic transfer magnetic resonance imaging of acute cerebral ischemia in the rat. *J. Cereb. Blood Flow Metab.* **22**, 547–558 (2002).
26. Ewing, J.R. *et al.* T_1 and magnetization transfer at 7 Tesla in acute ischemic infarct in the rat. *Magn. Reson. Med.* **41**, 696–705 (1999).
27. Hakumaki, J.M. & Kauppinen, R.A. ^{1}H NMR visible lipids in the life and death of cells. *TIBS* **25**, 357–362 (2000).